frontiers | Frontiers in Mechanical Engineering

TYPE Methods
PUBLISHED 23 November 2023
DOI 10.3389/fmech.2023.1194217

OPEN ACCESS

EDITED BY
Fuyin Ma,
School of Mechanical Engineering, Xi'an Jiaotong University, China

REVIEWED BY
Haijun Sun,
Nanchang Hangkong University, China
Yang Liu,
National University of Singapore, Singapore
Liu Bing,
Northwestern Polytechnical University, China

*CORRESPONDENCE
Liu Junli,
liujunliedu@126.com

RECEIVED 26 March 2023
ACCEPTED 11 April 2023
PUBLISHED 23 November 2023

CITATION
Zhang Y, Wu Y, Cao X, Liu Y, Sun Y, Yang J and Junli L (2023), Numerical simulation study on the effects of liquid water atomization on the flow field and performance of aluminum-based water ramjet engines.
Front. Mech. Eng 9:1194217.
doi: 10.3389/fmech.2023.1194217

Numerical simulation study on the effects of liquid water atomization on the flow field and performance of aluminum-based water ramjet engines

Yuntian Zhang[1], Yunkai Wu[1], Xiwei Cao[2], Yuanshu Liu[1], Yongqiang Sun[2], Jing Yang[1] and Liu Junli[1]*

[1]State Key Laboratory for Strength and Vibration of Mechanical Structures, Shaanxi Engineering Laboratory for Vibration Control of Aerospace Structures, School of Aerospace, Xi'an Jiaotong University, Xi'an, China, [2]Beijing Institute of Astronautical Systems Engineering, Beijing, China

In order to investigate the effects of different water inlet droplet diameters on the performance of aluminum-based water ramjet engines, the internal flow field of the engine was analyzed through numerical simulation. The results showed that by selecting a suitable water droplet diameter at the water inlet and controlling the time required for water droplet evaporation and heat absorption, the working range of aluminum-water combustion reaction can be expanded and the specific impulse of the engine can be increased. In engine design and practical application, the design of the water injection nozzle upstream of the engine is critical, and the droplet diameter at the water inlet should be controlled within a suitable range. A diameter that is too large will reduce the evaporation efficiency and hinder the further diffusion of combustion reaction. Droplet sizes that are too small will rapidly evaporate, causing the temperature in the flow field to decrease rapidly, leading to a large range of low-temperature regions in the main reaction zone of the combustion chamber, thereby reducing the overall aluminum-water reaction rate of the engine. In addition, the variation of droplet diameter in the downstream water atomization nozzle has little effect on the aluminum-water reaction in the main combustion zone. However, reducing the droplet diameter can facilitate the downstream diffusion of the combustion reaction, further expanding the combustion range and increasing the specific impulse. Furthermore, it can also reduce the temperature near the wall, which is beneficial for reducing the overall thermal protection requirements of the engine.

KEYWORDS

water ramjet engine, atomization, water droplet diameter, evaporation rate, numerical simulation

1 Introduction

With the development of ship technology and the continuous improvement of various detection and interception measures, old torpedoes with slow speed and short range are difficult to play a major role. Therefore, military powers around the world are striving to develop advanced torpedoes with high speed and long range. Russian experts pointed out that only the high-efficiency jet propulsion system using combustion metal fuel and seawater as the oxidant is the best way for underwater vessels to achieve high-speed propulsion. In

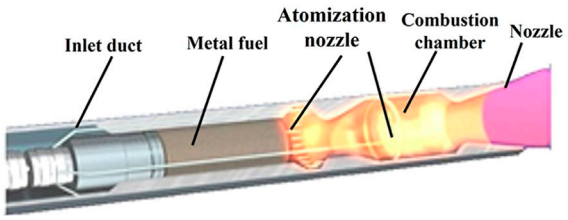

FIGURE 1
3D schematic diagram of the structure of the water stamping engine.

addition to Russia, military powers such as the United States and Germany are also researching various ultra-high-speed underwater weapons, including water ramjet engines and metal-water reaction fuels and related technologies.

The metal/water reaction ramjet engine is a new type of underwater propulsion device that uses high-energy reactive metal (aluminum, magnesium) as fuel and external seawater as oxidant and main working medium. The water ramjet engine utilizes the internal filled metal fuel and external seawater oxidant to generate the required thrust when the engine operates underwater, with advantages such as high specific impulse, simple structure, and high energy density. The water ramjet engine mainly consists of inlet duct, atomization nozzle, combustion chamber and nozzle, as shown in Figure 1. In the working process of the engine, external seawater is introduced into the combustion chamber through the inlet duct and inlet pipeline by means of the atomization nozzle, and water reacts vigorously with the metal-based fuel in the combustion chamber to produce high-temperature and high-pressure combustion gas, which is then expelled from the nozzle to generate thrust.

Due to the high volumetric heat value of metal fuels and the absence of oxidizer requirements, the water jet propulsion system utilizing metal fuels possesses a higher energy density and specific impulse compared to conventional solid rocket engines (Risha, 2006; He et al., 2022). In addition, the water jet propulsion system has the advantages of simple structure and high reliability, making it an ideal power source for high-speed and long-range underwater vehicles (Kiely, 1994). Among the high-energy metals, aluminum is often selected as the fuel for water jet propulsion systems due to its high volumetric energy density, good economic efficiency, and convenient storage (Kiely, 1994; Liu et al., 2018). This choice fully exploits the performance advantages of the water jet propulsion system.

As early as the last century, Branstetter et al. (1951) conducted the first research on aluminum metal as a propellant for water ramjet engines, and the results showed that metal aluminum could burn stably in a particulate state in the combustion chamber. In the early 21st century, relevant research institutions in the United States (Undersea Weapons Technologies, 2003) achieved underwater high-speed propulsion by using the reaction between water and aluminum metal fuel.

Compared to foreign research, the study of water-jet propulsion engines in China started relatively late. In the late 20th century, Fang et al. (2005) conducted tracking research on the relevant technology of water-jet propulsion engines. Through three-dimensional numerical simulation, they found that the performance of a water-jet propulsion engine using secondary water injection is superior to that of single water injection, and the water-to-fuel ratio needs to be reasonably allocated. Miao et al. (2005); Miao et al. (2007) improved the metal particle combustion model and concluded that the diameter of water droplet atomization has a significant impact on water evaporation, but has little effect on the chemical reaction between aluminum and water. Chang et al. (2021) conducted a two-dimensional numerical simulation of the flow field inside an aluminum-based metal water-jet propulsion engine and obtained the distribution of relevant parameters. (Li et al. (2022) set up a bluff body flame stabilizer in the combustion chamber of the water-jet propulsion engine to investigate the effect of changes in the configuration parameters of the flame stabilizer on the flow field characteristics in the combustion chamber. The results showed that when the height of the flame stabilizer relative to the gas inlet remained unchanged, the optimal performance of the water-jet propulsion engine was obtained when the distance from the flame stabilizer to the first water inlet was half the distance from the head of the flame stabilizer to the gas inlet. The internal combustion of a metal-based water-jet propulsion engine involves a series of complex physical and chemical processes such as two-phase turbulence, droplet evaporation, powder particle melting and sublimation, gas component diffusion, combustion chemical reactions, and solid surface chemical reactions. The mechanism is complex, which poses great difficulties for its related development and manufacture. Although scholars at home and abroad have conducted research on metal-based water-jet propulsion engines, the current research is still relatively preliminary, mainly focusing on the design of engine schemes. In a water-jet propulsion engine based on metal powder fuel, the water as an oxidant has an important impact on the mixing and stable combustion of the engine fuel through the atomization performance of the injector. Previous studies have paid less attention to the impact of atomization characteristics on the water-jet propulsion engine, and usually ignore the droplet diameter distribution in numerical simulation research, only considering single droplet diameter calculation, which cannot effectively reflect the engine performance. Therefore, this paper conducts numerical simulation research on the influence of liquid water injection characteristics on metal-based water-jet propulsion engines, and explores the impact of the droplet size of the first and second water injection ports on the flow field structure inside the aluminum-based metal fuel water-jet propulsion engine and its corresponding engine performance.

2 Material and methods

Due to the complexity of the multiphase turbulent combustion, aluminum particle oxidation reaction, and water droplet evaporation process inside the aluminum-based water-cooled engine, it is currently impossible to accurately simulate all the physical processes involved. Therefore, in numerical simulation, the flow field calculation must be carried out, and the combustion

products generated by the combustion reaction in the combustion chamber are assumed to be a thermally perfect gas, satisfying the equation of state for a perfect gas.

2.1 Governing equations

In this paper, the finite volume method is used to solve the Navier-Stokes equations. The continuous phase (gas phase) governing equations and the discrete phase (liquid phase, metal particle phase) governing equations are established, and the coupling between the discrete phase and the gas phase is represented by the source term of gas/discrete phase interaction in the continuous phase governing equations. The gas phase governing equations are described in the Eulerian coordinate system, while the discrete phase governing equations are described in the Lagrangian coordinate system. The governing equations for the combustion flow field with multiple components and chemical reactions are as follows:

$$\frac{\partial \rho}{\partial t} + \frac{\partial}{\partial x_j}\left(\rho u_j\right) = S_m \tag{1}$$

$$\frac{\partial}{\partial t}\left(\rho u_i\right) + \frac{\partial}{\partial x_j}\left(\rho u_i u_j\right) = -\frac{\partial}{\partial x_j}\left(\delta_{ij} p\right) + \frac{\partial \tau_{ij}}{\partial x_j} + S_{ui} \tag{2}$$

$$\frac{\partial}{\partial t}\left(\rho E\right) + \frac{\partial}{\partial x_j}\left[\left(\rho E + p\right)u_j\right] = \frac{\partial}{\partial x_j}\left(u_i \tau_{ij} - q_j\right) + S_h \tag{3}$$

$$\frac{\partial}{\partial t}\left(\rho Y_m\right) + \frac{\partial}{\partial x_j}\left[\rho Y_m u_j + J_{j,m}\right] = R_m + S_{Ym} \tag{4}$$

They are the equations for mass transport, momentum transport, energy transport, and component transport, respectively.

Viscous shear stress is

$$\tau_{ij} = \mu\left[\left(\frac{\partial u_i}{dx_j} + \frac{\partial u_j}{dx_i}\right) - \frac{2}{3}\delta_{ij}\frac{\partial u_k}{dx_k}\right] \tag{5}$$

In the equation, μ is the molecular dynamic viscosity coefficient, which can be expressed as $\mu = \mu l + \mu t$. Here, μl is the laminar viscosity coefficient, which is given by the Sutherland formula as a polynomial function of temperature, and μt is the turbulent viscosity coefficient, which is provided by the turbulent flow model. The δij is the Kronecker delta.

In this study, the κ-ω Menter SST model was used as the turbulence model. The Reynolds-averaged form of the κ-ω Menter SST turbulence model was employed. This model uses the Wilcox κ-ω model near the wall, and the κ-ε model in the boundary layer edge and free shear layer. A blending function is introduced to transition between the two models, which is designed specifically for near-wall flows, taking advantage of the κ-ε model's ability to handle free flows and the κ-ω model's capability to address wall-bounded flow issues. Therefore, it has certain advantages for computing combustion flows. For a detailed description of this turbulence model, please refer to reference (Magnussen, 1981), and it will not be repeated here.

2.2 Discreate phase model

The discrete phase is distributed in the continuous phase composed of gas, and the Lagrangian method is used to track the motion of the discrete phase in the flow field, and to calculate the trajectory and heat and mass transfer process of the discrete phase. The movement law of the discrete phase and the characteristics of the gas phase flow field are obtained by iterative calculation through the coupling between the two phases after the entire flow field is stabilized. The velocity of the discrete phase is obtained by solving the differential equation of the force acting on the discrete phase droplets or particles in the Lagrangian coordinate system through integration, and the force acting on the droplets or particles equals their inertia, as shown below (in the x-direction of the Cartesian coordinate system):

$$\frac{du_p}{dt} = F_D\left(u - u_p\right) + \frac{g_x\left(\rho_p - \rho\right)}{\rho_p} + F_x \tag{6}$$

In the equation, gx represents the gravitational acceleration, Fx represents the additional force per unit mass acting on the droplet (particle), and F_D represents the unit mass drag force acting on the droplet (particle). For a detailed description of the discrete phase model and its parameters, refer to reference (Liu et al., 2019). The evaporation of water droplets and particles is modeled using a droplet evaporation model described in reference (Ranz and Marshall, 1952). Due to space limitations, this paper does not provide a detailed description of these models.

2.3 Combustion and particle reaction kinetics model

In this study, the eddy dissipation concept (EDC) model was chosen to simulate the combustion process of aluminum-based metal fuel (Magnussen, 1981; Parente et al., 2016). The EDC model is based on the eddy dissipation model, assuming that chemical reactions occur in fine eddies, and the reaction time is jointly controlled by the time required for chemical reactions themselves and the existence time of small eddies. The EDC model includes a detailed chemical reaction mechanism in turbulent reactions, so it can simultaneously consider the effects of chemical reaction kinetics and turbulence on chemical reaction rates. The surface reaction model for particles (Liu et al., 2019) was used to simulate the combustion of aluminum-based metal fuel in a water ramjet engine in this study. This model takes into account both heterogeneous surface combustion and gas-phase combustion. The reaction process of aluminum-water mainly consists of two steps:

1. Reaction between aluminum vapor and water vapor produced when aluminum particles are heated to the evaporation temperature (937 K):

$$2\mathrm{Al(g)} + 3\mathrm{H_2O(g)} \rightarrow \mathrm{Al_2O_3(g)} + 3\mathrm{H_2}\uparrow$$

2. Reaction between aluminum particles and water vapor:

$$2\mathrm{Al(s)} + 3\mathrm{H_2O(g)} \rightarrow \mathrm{Al_2O_3(s)} + 3\mathrm{H_2}\uparrow$$

2.4 Physical model

The aluminum-based fuel water-ramjet engine designed in this study is shown in Figure 2. The engine adopts a two-stage liquid water injection method and head injection of metal powder propellant for mixing and reacting in the combustion chamber to produce thrust.

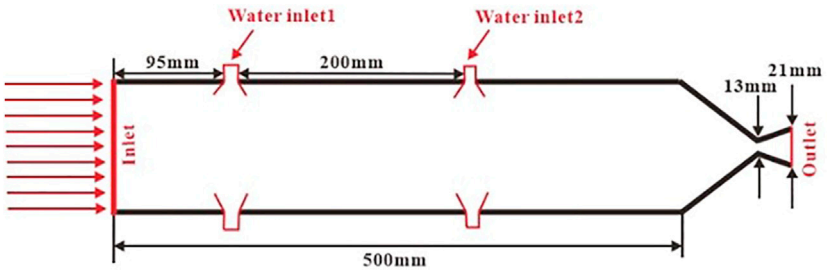

FIGURE 2
Structural drawing of water ramjet.

TABLE 1 Parameter distribution of atomized water droplet diameter.

Case	Diameter of atomized water droplets at the primary water inlet/μm	Diameter of atomized water droplets at the secondary water inlet/μm
1	10	30
2	30	30
3	50	30
4	30	10
5	30	50

The first stage liquid water injector (referred to as the primary inlet) located near the head of the engine is at a distance of L_1 = 95 mm from the head of the water-ramjet engine, and the second stage liquid water injector (referred to as the secondary inlet) located near the downstream end is at a distance of L_2 = 305 mm from the head of the engine.

2.5 Operating conditions and boundary conditions

To investigate the effects of different droplet diameters at the 1st and 2nd water injection ports on the flow field of the aluminum-based metal fuel water-ramjet engine, we designed five different operating conditions as shown in Table 1. In cases 1–3, the droplet diameter at the 2nd water injection port was fixed at 30 μm, while the droplet diameters at the 1st water injection port were 50 μm, 30 μm, and 10 μm, respectively, to analyze the influence of the 1st water injection port droplet diameter on the flow field. In cases 3–5, the droplet diameter at the 1st water injection port was fixed at 30 μm, while the droplet diameters at the 2nd water injection port were 50 μm, 30 μm, and 10 μm, respectively, to analyze the influence of the 2nd water injection port droplet diameter on the flow field. Based on the aforementioned physical configuration of the engine and its underwater working conditions, the boundary conditions were set as follows:

1. The 1st water injection port used a mass flow inlet, with a water-to-fuel ratio of 0.85 and a temperature of 300 K.

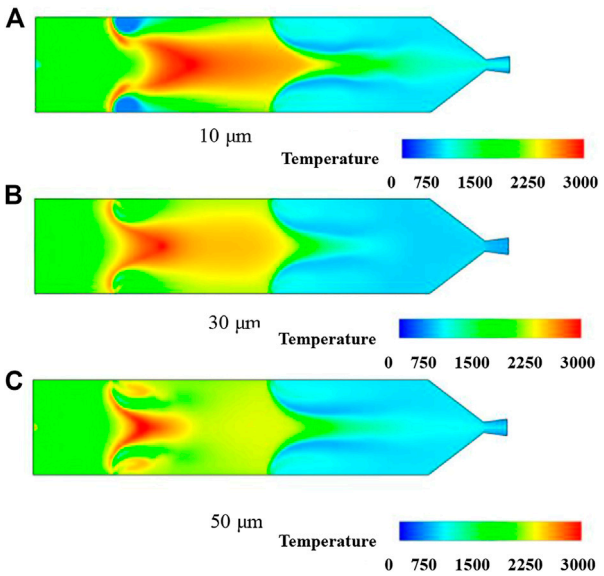

FIGURE 3
Temperature distribution of flow field in water ramjet [**(A)** case 1, **(B)** case 2, **(C)** case 3].

2. The 2nd water injection port used a mass flow inlet, with a water-to-fuel ratio of 1.7 and a temperature of 300 K.
3. The mass fraction of solid aluminum powder in the aluminum-based metal fuel was 80%, and the total mass flow rate was 0.12 kg/s, of which 40% of the total mass was volatile.

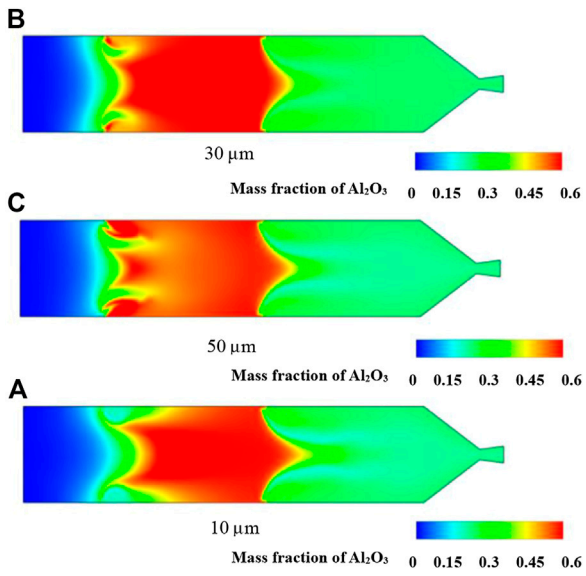

FIGURE 4
Mass fraction distribution of Al_2O_3 [**(A)** case 1, **(B)** case 2, **(C)** case 3].

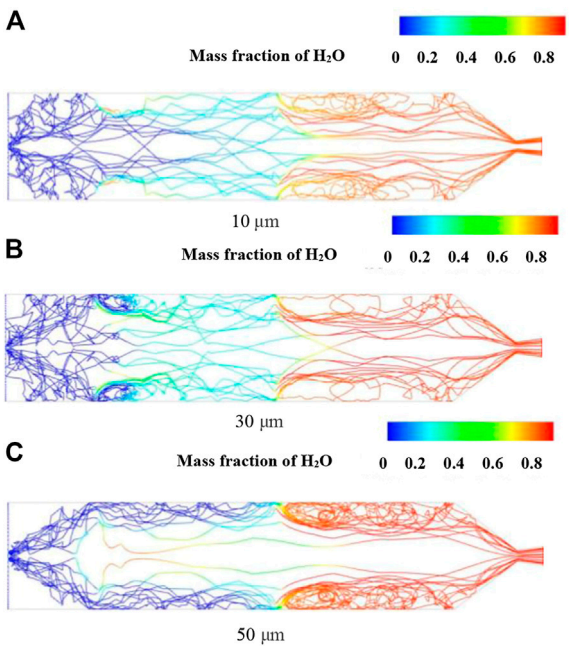

FIGURE 5
Variation chart of water droplet mass with trajectory [**(A)** case 1, **(B)** case 2, **(C)** case 3].

4. The wall was set to be adiabatic.
5. The outlet was a pressure outlet.

3 Results

3.1 Effect of 1st inlet droplet size

Firstly, the effect of 1st inlet droplet size was investigated under the conditions where the droplet size of the 2nd inlet was fixed at 30 μm and the droplet size of the 1st inlet was set to 10 μm, 30 μm, and 50 μm for cases 1–3, respectively. Figure 3 shows the temperature distribution inside the water-jet propulsion engine for different droplet sizes of the 1st inlet. It can be observed that when the droplet size of the 1st inlet is 10 μm, a clear low-temperature area appears due to the evaporation and endothermic effect of water droplets at the 1st inlet. The high-temperature region generated by combustion is concentrated between the 1st and 2nd inlets, where the reaction between aluminum fuel and water mainly takes place. Since there is still a small amount of unreacted aluminum fuel, the engine uses the 2nd inlet to supplement the working fluid. Under the premise of ensuring efficient combustion reaction in the combustion chamber, the evaporation and endothermic effect of a large amount of low-temperature droplets are utilized to cool down the internal flow field and provide high-temperature protection.

When the diameter of water droplets at the first water injection port increased to 30 μm (case 2), the low-temperature region at the first injection port disappeared. This is mainly because with the increase of water droplet diameter, the contact area between water droplets and aluminum fuel per unit mass decreases, leading to longer evaporation time and reduced heat absorption of water droplets in the reaction zone. As a result, the main combustion region moves closer to the center of the combustion chamber. However, due to the slow evaporation process of water droplets, there was no rapid temperature drop phenomenon as in case 1, which better promotes the progress of the aluminum-water reaction and enlarges the main reaction zone between the first and second water injection ports. For case 3 with a liquid water droplet diameter of 50 μm, the further increase of droplet diameter results in decreased evaporation efficiency, increased two-phase flow losses, and reduced range of high-temperature region, which is not conducive to the further propagation of the reaction.

Figure 4 shows the distribution of Al_2O_3 mass fraction in the flow field of the water-injected engine under operating conditions 1–3. In case 1, due to the rapid evaporation and heat absorption of water droplets, the Al_2O_3 concentration near the first injection port is relatively low, and mainly concentrates in the center of the combustion chamber and spreads to both sides. In case 3, the larger droplet diameter (50 μm) requires a longer evaporation time, resulting in lower product concentration in the central region. When a droplet diameter of 30 μm is used for injection (condition 2), the amount and distribution of product Al_2O_3 are the largest, indicating a more intense aluminum-water reaction at this droplet size.

Figure 5 shows the variation of water droplet mass along the trajectory under cases 1–3. It can be seen that the evaporation efficiency of water droplets has a significant impact with the change of droplet diameter. Water droplets under cases 1-2 can evaporate in a short time, allowing for effective mixing combustion with aluminum fuel in the main reaction zone between the first and second water inlets. However, under the condition of large droplet diameter in case 3, the slow evaporation process leads to insufficient time for effective mixing combustion between water droplets and

10.3389/fmech.2023.1194217

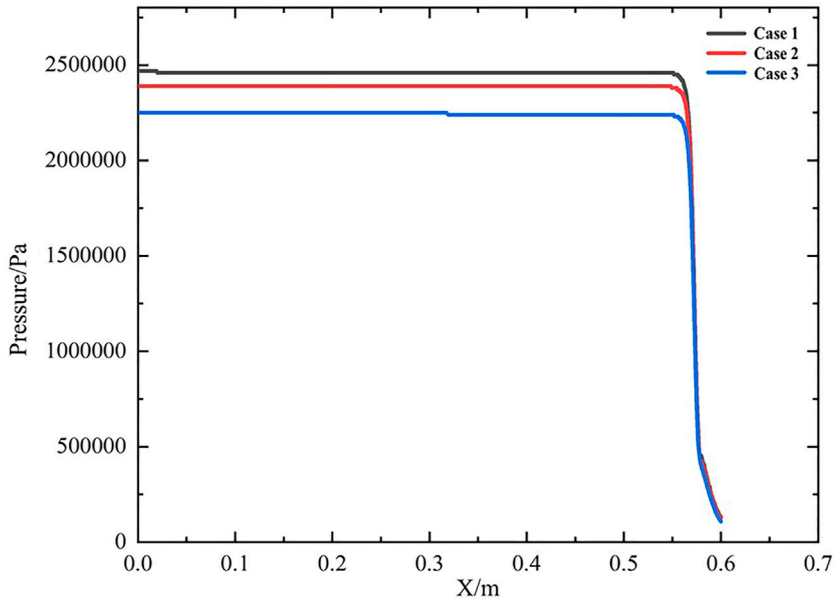

FIGURE 6
Pressure curve of flow field in water ramjet.

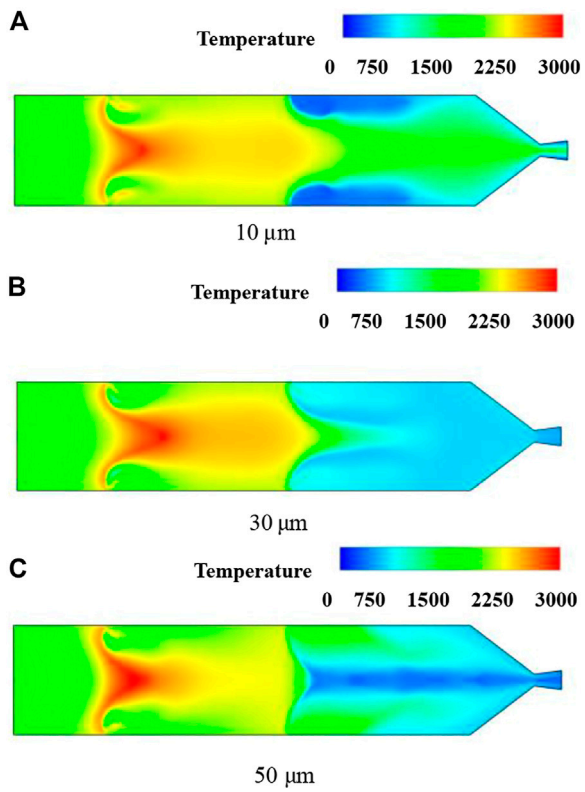

FIGURE 7
Temperature distribution of flow field in water ramjet [**(A)** case 4, **(B)** case 2, **(C)** case 5].

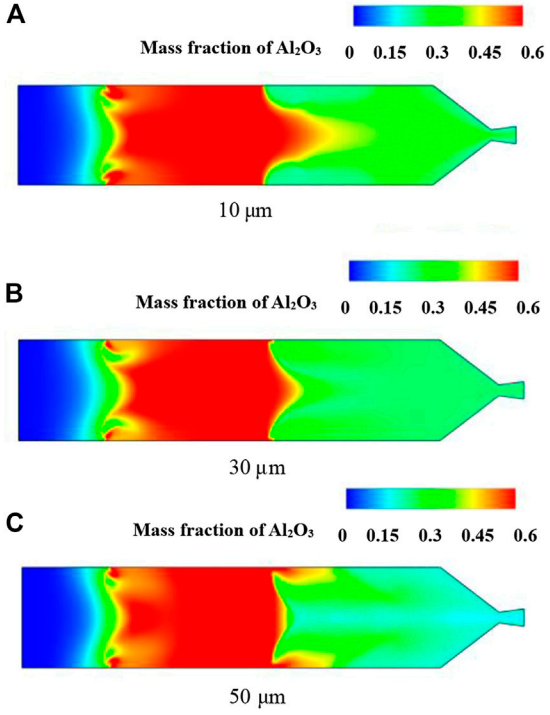

FIGURE 8
Mass fraction distribution of Al_2O_3 [**(A)** case 4, **(B)** case 2, **(C)** case 5].

aluminum fuel, resulting in the water droplets mainly existing near the combustion chamber wall and more concentrated between the second water inlet and the nozzle outlet, thereby affecting the combustion reaction.

Figure 6 shows the axial pressure variation curve under cases 1–3. It can be seen that the overall pressure along the axial direction of the combustion chamber of the water-assisted stamping engine is relatively stable. The water, as an oxidizer, is injected twice along the axial direction, which has a certain influence on the pressure variation of the combustion chamber, but the overall change is not significant. As the diameter of the water droplets at the first water inlet increases, the pressure value of the combustion chamber of the water-assisted stamping engine gradually decreases, resulting in a decrease in thrust.

3.2 Effect of secondary inlet atomization diameter

In this section, cases 4-5 are used to investigate the effects of atomization diameter of the second water injection port on the flow field structure and working characteristics of the water-jet-assisted engine when the atomization diameter of the first water injection port remains unchanged.

Figures 7, 8 show the temperature distribution and the distribution of Al_2O_3 mass fraction in the flow field of the water-jet-assisted engine under different atomization diameters of the second water injection port (with the atomization diameter of the first water injection port kept at 30 μm for conditions 2, 4, and 5). It can be seen that the change in the atomization diameter of the second water injection port has a relatively small impact on the main combustion zone of the water-jet-assisted engine compared with the change in the atomization diameter of the first water injection port. This is mainly because before reaching the vicinity of the second water injection port, aluminum and water vapor have already undergone relatively sufficient mixing and reaction, leading to a large consumption of aluminum particles. Therefore, the water-to-fuel ratio is relatively high near the second water injection port, and the injection of water causes the high-temperature mixed gas to rapidly cool down, resulting in a decrease in its contribution to the main combustion zone near the second water injection port.

When the diameter of the water droplets injected into the second water inlet is 10 μm, a large low-temperature area appears near the second water inlet due to the rapid evaporation and heat absorption. At this time, the temperature near the wall is 400 K. Water vapor diffuses into the central area of the combustion chamber and mixes with unreacted aluminum metal, expanding the area of the core reaction zone. As the diameter of the water droplets increases, the temperature in the near-wall area between the second water inlet and the downstream nozzle gradually increases. When the diameter of the water droplets is 50 μm, the temperature near the wall reaches 1500 K. This indicates that the water injected from the second water inlet is unable to cool the high-temperature zone of the main combustion generated by the water injected from the first water inlet in a timely manner, and puts higher demands on the thermal protection of the water injection engine. At the same time, a large droplet diameter makes it impossible to evaporate the droplets into water vapor quickly, causing the low-temperature area to shift downward and reducing the Al_2O_3 content in the center of the combustion chamber, which in turn reduces the combustion efficiency of aluminum metal.

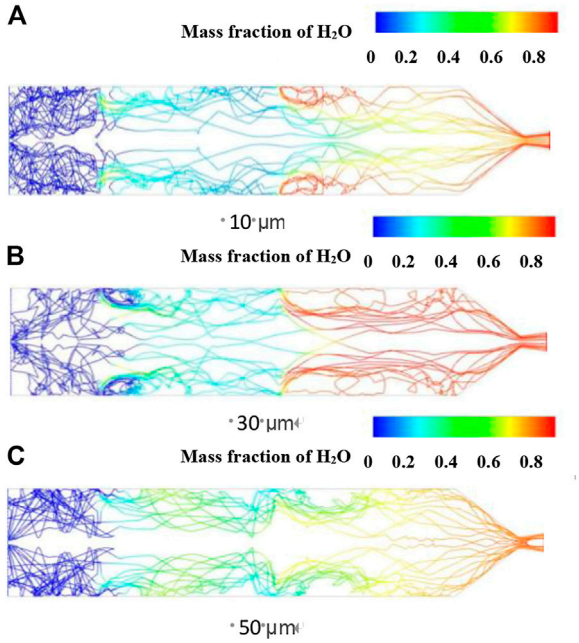

FIGURE 9
Variation chart of water droplet mass with trajectory [**(A)** case 4, **(B)** case 2, **(C)** case 5].

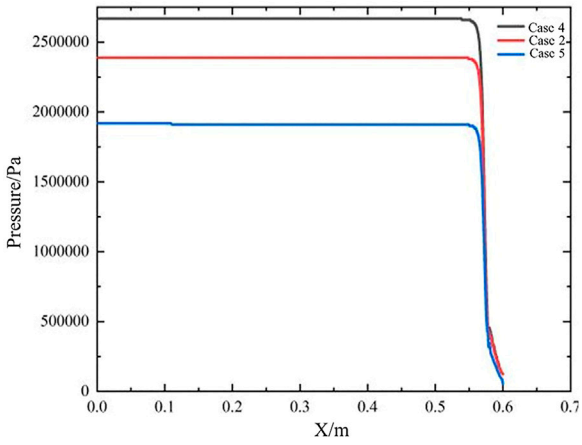

FIGURE 10
Pressure curve of flow field in water ramjet.

Figure 9 shows the variation of the mass fraction of water droplets along their trajectories under different diameters of water droplets injected from the second water inlet (cases 2, 4, and 5). As the diameter of the atomized water droplets decreases, the residence time of water droplets in the central area increases, so the consumption rate of water in the main reaction zone of the

TABLE 2 Dimensionless specific impulse of water ramjet under different working conditions.

Case	Dimensionless specific impulse
1	0.83
2	0.79
3	0.75
4	0.9
5	0.6

combustion chamber increases with the decrease in the diameter of the water droplets. For condition 5, where the diameter of the water droplets injected from the second water inlet is 50 μm, the water vapor content in the central area of the downstream combustion chamber drops significantly. This indicates that a large atomized droplet diameter slows down the heat absorption and evaporation process of the water droplets, making water vapor more concentrated near the injection nozzle, and thus preventing the water vapor from reacting with aluminum in a timely manner, resulting in a large low-temperature zone in the central area of the combustion chamber and reducing the overall combustion efficiency and engine performance. On the other hand, when the diameter of the droplets injected is smaller (case 4), the water vapor can linger in the central area of the combustion chamber for a long time, supplementing oxidants for the aluminum-water reaction, promoting the reaction between the aluminum-based fuel and water, expanding the combustion range, and thereby improving the overall performance of the engine.

Figure 10 shows the variation of axial pressure in the engine for different 2nd injection water droplet diameters, and it can be seen from the five operating conditions that decreasing the diameter of atomized water droplets can increase the pressure in the combustion chamber. Furthermore, the diameter of the atomized water droplets at the 2nd water inlet has a greater impact on chamber pressure than that at the 1st water inlet, because the water-to-fuel ratio at the 2nd water inlet is much higher than that at the 1st water inlet, and the amount of heat absorbed by water droplet evaporation is greater, which has a greater effect on the flow field inside the combustion chamber. Under operating condition 4, the highest pressure can reach 2.7 MPa, indicating that the combination of a 30 μm water droplet diameter at the 1st injection port and a 10 μm water droplet diameter at the 2nd injection port results in the highest combustion intensity for the water jet engine. However, for operating condition 5, the large diameter of atomized water droplets downstream of the combustion chamber results in slow heat absorption and evaporation of water droplets, which cannot supplement the gas volume in a timely manner, leading to a decrease in the combustion efficiency of the aluminum-water reaction.

Table 2 presents the dimensionless specific impulse of the steady-state internal flow field of the water-impulse engine under five different operating conditions. It can be observed that the dimensionless specific impulse is highest under condition 4. Comparing case 1 and case 2, although the specific impulse slightly increases, the temperature distribution and the mass fraction distribution of Al_2O_3 product shown in Figures 3, 4 indicate that the rapid evaporation of small droplets from the 1st injection port leads to a rapid decrease in the flow field temperature, causing a large area of low-temperature region in the main reaction zone of the combustion chamber, reducing the reaction rate of aluminum-water mixture and decreasing the high-temperature reaction zone. Therefore, the selection of a moderate droplet size of 30 μm at the 1st injection port is more appropriate. Conversely, cases 3 and 5 exhibit the lowest specific impulse, indicating that excessively large droplet sizes at the 2nd injection port significantly reduce combustion efficiency and subsequently engine performance.

In summary, there exists an optimal selection of droplet sizes for the 1st and 2nd injection ports in the water-impulse engine, which can achieve the best combustion performance and operational efficiency.

4 Discussion

In this study, numerical simulations were performed to investigate the flow field structure and engine performance of an aluminum-based water-jet engine model's combustion chamber, and the effect of different droplet diameters of the first and second water injection ports on the flow field was analyzed. The results indicate that: 1) For water-jet engines, the droplet diameter of liquid water injected into the combustion chamber has a significant impact on the structure of the main heat release zone and engine performance. As the droplet diameter increases, the overall evaporation time of water droplets in the combustion chamber will increase, which will have an adverse effect on their mixing with metal particles and combustion. 2) The droplet diameter of the first water injection port needs to be maintained within an appropriate range. If the diameter is too large, the evaporation efficiency will be further reduced, the two-phase flow loss will increase, and the range of the high-temperature region will decrease, which is not conducive to the diffusion of the high-temperature reaction zone. If the droplet diameter is too small, the liquid water will quickly evaporate, leading to a rapid decrease in the temperature of the main heat release zone in the combustion chamber, which will reduce the rate of aluminum-water reaction, decrease the high-temperature reaction zone, and thus affect the engine's combustion chamber pressure and performance improvement. 3) The droplet diameter of the second water injection port has a smaller impact on the aluminum-water reaction in the main combustion zone. However, reducing the injection diameter of this water injection port is not only conducive to the downstream diffusion of the high-temperature reaction zone, further expanding the combustion range and increasing specific impulse but also reduces the temperature near the wall, which is beneficial to thermal protection. Therefore, for the metal-based fuel water-jet engine studied in this paper, due to the different effects of the first and second water injection ports on the combustion reaction flow field structure and performance, the optimal injection droplet diameter of liquid water also varies. The selection should be matched according to the engine's combustion and thermal protection performance requirements.

Data availability statement

The original contributions presented in the study are included in the article/supplementary material, further inquiries can be directed to the corresponding author.

Author contributions

YZ, YW, and XC performed the data analysis; YZ and LJ performed the formal analysis; YL performed the validation; YS and JY wrote the manuscript.

Funding

This work was supported by the China Postdoctoral Science Foundation (Grant Nos 2019TQ0246 and 2019M663734), the National Science Basic Research Program of Shaanxi (Program No. 2022JM-231), the Natural Science Foundation of Shaanxi Province [2021JQ-358].

Conflict of interest

The authors declare that the research was conducted in the absence of any commercial or financial relationships that could be construed as a potential conflict of interest.

The handling editor FM declared a shared affiliation with the authors at the time of review.

Publisher's note

References

Branstetter, J. R., Lord, A. M., and Gerstein, M. (1951). Combustion properties of aluminum as ramjet fuel [J]. *Tech. Rep. Archive Image Libr*, 37. https://digital.library.unt.edu/ark:/67531/metadc58917/.

Chang, H., Xu, N., Zheng, L., Pu, X., Hu, Y., and Huang, H. (2021). Numerical simulation of internal flow field in an aluminum-based metal-fuel water ramjet engine [J]. *Eng. J. Wuhan Univ.* 54 (02), 144–148.

Fang, L., Weihua, Z., Zhang, W., Yang, S.-Q., and Xia, Z.-X. (2005). A preliminary research on the performance of hydroreactive aluminium metal fuel[J]. *J. Natl. Univ. Def. Technol.* (04), 4–7. http://journal.nudt.edu.cn/gfkjdxxb/ch/reader/view_abstract.aspx?file_no=200504002&flag=1.

He, Z., Gao, Z., Gu, X., Sun, X., and Liu, A. (2022). Dimensional design and simulation of water inlet pipeline for water ramjet[J]. *J. Solid Rocket Technol.* 45 (02), 194–199.

Kiely, D. H. (1994). *Review of underwater thermal propulsion[C] AIAA 94-2837*, 21–25.

Li, S., Xiang, M., Yang, X., Xie, Z., and Zhang, W. (2022). Effect of flame stabilizer relative parameters on combustion and flow field in water ramjet[J]. *J. Aerosp. Power* 36 (10), 2230–2240.

Liu, K., Luo, P., and Xiong, C. (2018). Research development of hydroreactive metal fuel used for water-ramjet engine[J]. *Hot Work. Technol.* 47 (10), 18–21.

Liu, P., Chang, H., Li, S., and Wang, W. (2019). Numerical simulation of distributed combustion of the aluminized composite propellant[J]. *J. Solid Rocket Technol.* 41 (02), 156–161.

Magnussen, B. F. (1981). *On the structure of turbulence and a generalized eddy dissipation concept for chemical reactions in turbulent flow[R]*. AIAA 81-37570.

Miao, W., Xia, Z., Fang, D., and Han, C. (2007). Numerical simulation on 3D internal flow field of metal/water reaction ramjet[J]. *J. Solid Rocket Technol.* 30 (02), 102–105.

Miao, W., Xia, Z., Guo, J., Hu, J., Zhao, J., Luo, Z., et al. (2005). Thermodynamic calculation for the water ramjet[J]. *J. Propuls. Technol.* 26 (06), 85–88.

Parente, A., Malik, M. R., Contino, F., Cuoci, A., and Dally, B. B. (2016). Extension of the Eddy Dissipation Concept for turbulence/chemistry interactions to MILD combustion. *Fuel* 163 (1), 98–111. doi:10.1016/j.fuel.2015.09.020

Ranz, W. E., and Marshall, W. R. (1952). Evaporation from drops, Part I[J]. *Chem. Eng. Prog.* 48 (3), 141–146.

Risha, G. A. (2006). *Combustion of aluminum particles with steam and liquid water [R]*. AIAA 2006-1154.

Undersea Weapons Technologies (2003). *An assessment of undersea weapons science and technology*. https://nap.nationalacademies.org/catalog/9863/an-assessment-of-undersea-weapons-science-and-technology.